Ferromagnetic quantum critical phenomena in single-crystalline SrCo$_2$(Ge$_{1-x}$P$_x$)$_2$

K. Moriyama [*], C. Michioka, H. Ueda, and K. Yoshimura [†]

Department of Chemistry, Graduate School of Science, Kyoto University, Kyoto 606-8502, Japan

Single crystals of SrCo$_2$(Ge$_{1-x}$P$_x$)$_2$ were grown using a self-flux method, and their physical properties were investigated by means of magnetization and specific-heat measurements. Although the compounds near both ends of x exhibit paramagnetism, those with $0.39 \leqslant x \leqslant 0.58$ exhibit ferromagnetism at low temperatures. The analysis of critical exponents and spin fluctuations revealed a weak itinerant ferromagnetic character. It is found that an intermediate phase exists for a wide range of composition between the collapsed tetragonal and the uncollapsed tetragonal phases, which causes ferromagnetic quantum critical phenomena in SrCo$_2$(Ge$_{1-x}$P$_x$)$_2$.

I. INTRODUCTION

The ThCr$_2$Si$_2$-type layered compounds AT_2X_2 (A = alkali metal, alkaline earth metal, lanthanoid, T = transition metal, X = crystallogen, pnictogen, chalcogen) have been extensively investigated since they exhibit a wide variety of anomalous physical properties, such as heavy-fermion superconductivity in CeCu$_2$Si$_2$ [1], high-T_c superconductivity in carrier-doped systems of BaFe$_2$As$_2$ [2,3] and itinerant-electron metamagnetic transition in SrCo$_2$P$_2$ [4]. AT_2X_2 consists of alternately stacked A and TX layers and is classified into two types depending on the presence of the X-X chemical bonds between neighboring TX layers: one is the collapsed tetragonal (cT) structure with the interlayer X-X bonds, the other is the uncollapsed tetragonal (ucT) structure without the bonds. The formation of the X-X bonds leads not only to a reduction of the interlayer distance, but also to a distortion of TX_4 tetrahedron, resulting in both a decrease in the lattice parameter c and an increase in the parameter a.

The structural transition between the cT and the ucT phases can lead to significant changes in physical properties. For EuCo$_2$P$_2$, whereas only the magnetic moment of Eu^{2+} exhibits helical ordering in the ucT phase at ambient pressure [5], a pressure-induced phase transition to the cT structure leads to both a valence shift in Eu and an antiferromagnetic ordering of Co moment [6]. According to the previous studies on magnetization for Sr$_{1-x}$Ca$_x$Co$_2$P$_2$, compounds in the ucT phase with $0 \leqslant x \leqslant 0.5$ exhibit exchange-enhanced Pauli paramagnetism down to low temperatures, whereas those in the cT phase with $0.6 \leqslant x \leqslant 1$ exhibit A-type antiferromagnetic ordering [4,7].

In the above cases, the structural and magnetic phases seem to be coincide. On the other hand, the characteristic magnetic phase diagram in SrCo$_2$(Ge$_{1-x}$P$_x$)$_2$ cannot be explained by the simple structural phase diagram consisting only of the cT and ucT phases. SrCo$_2$Ge$_2$ ($x = 0$) has the cT structure with a short interlayer Ge-Ge distance (2.88 Å), whereas SrCo$_2$P$_2$ ($x = 1$) has the ucT structure with a long interlayer

P-P distance (3.42 Å) [8]. According to the previous report on polycrystalline samples of SrCo$_2$(Ge$_{1-x}$P$_x$)$_2$, compounds in the cT phase with $0 \leqslant x < 0.325$ exhibit Pauli paramagnetism, and those in the ucT phase with $0.7 < x \leqslant 1$ exhibit exchange-enhanced Pauli paramagnetism, whereas only the compounds with $0.325 \leqslant x \leqslant 0.7$ exhibit ferromagnetism at low temperatures [9]. Although there have been several reports of ferromagnetism induced by substituting elements in nearly ferromagnetic metals, it is rare that such a ferromagnetic phase disappears again with further substitutions. In order to clarify the relationship between these anomalous properties and the crystal structure, further experiments and analysis of ferromagnetism are desired.

The modified Arrott plot method proposed by Arrott and Noaks is one of effective methods to characterize the feature of ferromagnetism [10]. Recently, critical exponents have been evaluated for two-dimensional itinerant ferromagnets, such as Fe$_{3-x}$GeTe$_2$ [11] and AlFe$_2$B$_2$ [12] using modified Arrott plots. The critical exponents provide information on the universality class of the magnetic phase transition, which is important to understand the nature of the magnetically ordered state. In addition, the magnetic properties in itinerant-electron ferromagnets, such as Y(Co$_{1-x}$Al$_x$)$_2$ [13–16], Sr$_{1-x}$Ca$_x$RuO$_3$ [17–19], FeGa$_{3-x}$Ge$_x$ [20–22], and LaCrGe$_3$ [23] have been quantitatively analyzed using the self-consistent renormalization (SCR) theory. In the SCR theory, the spectrum of the imaginary part of the dynamical magnetic susceptibility is approximately represented using a double Lorentz function [24]. The spin-fluctuation parameters T_A and T_0 are defined to represent the dispersion of the spectrum in the wave-number space and that in the frequency space, respectively. At finite temperatures, spin fluctuations are excited thermally according to the dynamical magnetic susceptibility. By self-consistently incorporating the effect of the mode-mode coupling between spin fluctuations into the magnetic susceptibility, one can explain typical features of weak ferromagnetism in an itinerant-electron system, such as the Curie-Weiss behavior of the magnetic susceptibility.

In this paper, we present the magnetic properties in single crystals of SrCo$_2$(Ge$_{1-x}$P$_x$)$_2$. We have grown single crystals

---
[*]moriyama.koudai.77c@kyoto-u.jp
[†]yoshimura.kazuyoshi.8e@kyoto-u.ac.jp

with a wide range of substitution ratio using a self-flux method and measured their magnetization and specific heat. We characterized the ferromagnetism in terms of critical exponents and spin fluctuations, and produced a detailed magnetic phase diagram. Our results suggest that an intermediate phase exists for a wide range of composition, which causes quantum critical phenomena in $SrCo_2(Ge_{1-x}P_x)_2$.

II. EXPERIMENTAL METHOD

Single-crystalline samples of $SrCo_2(Ge_{1-x}P_x)_2$ ($0 \leqslant x \leqslant 0.9$) were synthesized using a self-flux method. Starting materials consisting of Sr (99%), Co (99.9%), P (99.999%), and Ge (99.99%), with composition ratio of Sr:Co:P:Ge = 1-2.4:4:$2.5x_{nominal}$:5, were put into an alumina crucible and sealed into an evacuated fused quartz tube. The tube was heated to $1100\,^\circ$C, kept at this temperature for 15 h, and slowly cooled to $700\,^\circ$C at the rate of $2.5\,^\circ$C/h. Excess flux was removed by dilute hydrochloric acid. Single-crystalline samples of $SrCo_2P_2$ ($x = 1$) were obtained using a tin flux method [25]. In order to compare lattice constants, single crystals of $Ca_{1-x}Eu_xCo_2P_2$ were also synthesized using a tin flux method.

Elemental compositions of obtained crystals were checked using an energy dispersive x-ray (EDX) spectroscopy (Bruker) equipped to a scanning electron microscope (Hitachi). The x-ray diffraction (XRD) patterns of obtained single crystals were measured at room temperature using Miniflex600 (Rigaku) with Cu $K\alpha$ radiation. The crystallographic parameters were refined using POWDER CELL analysis [26].

The temperature and magnetic-field-dependent magnetizations M in single crystals of $SrCo_2(Ge_{1-x}P_x)_2$ were measured using a Quantum Design magnetic property measurement system at the Research Center for Low Temperature and Materials Sciences, Kyoto University. Heat-capacity measurements were performed using a Quantum Design physical property measurement system.

III. RESULTS AND DISCUSSION

A. Sample characterization

Using the self-flux method, platelike single crystals with a typical dimension of $0.5 \times 0.5 \times 0.05$ mm³ shown in the inset of Fig. 1(a) were obtained. Figure 1(a) shows the plots of the P content x determined using EDX measurements against the starting P content $x_{nominal}$. The composition of the crystals depends not only on $x_{nominal}$, but also on the starting ratio of Sr. Crystals with $x > 0.81$ were obtained under the condition of low Sr content. In the following discussion, x is defined as the P content determined using EDX measurements.

Figure 1(b) shows the normalized XRD patterns of $SrCo_2(Ge_{1-x}P_x)_2$ single crystals with the plate surface being perpendicular to the scattering vector. Only (00l) diffraction peaks were observed, which suggests that the surface is the ab plane. The composition dependence of the lattice parameters determined using the XRD measurements for powdered samples will be discussed in Sec. III F.

B. Magnetic properties

Figure 2(a) shows the temperature dependence of the magnetic susceptibility $\chi(T)$ in $SrCo_2(Ge_{1-x}P_x)_2$ single crystals
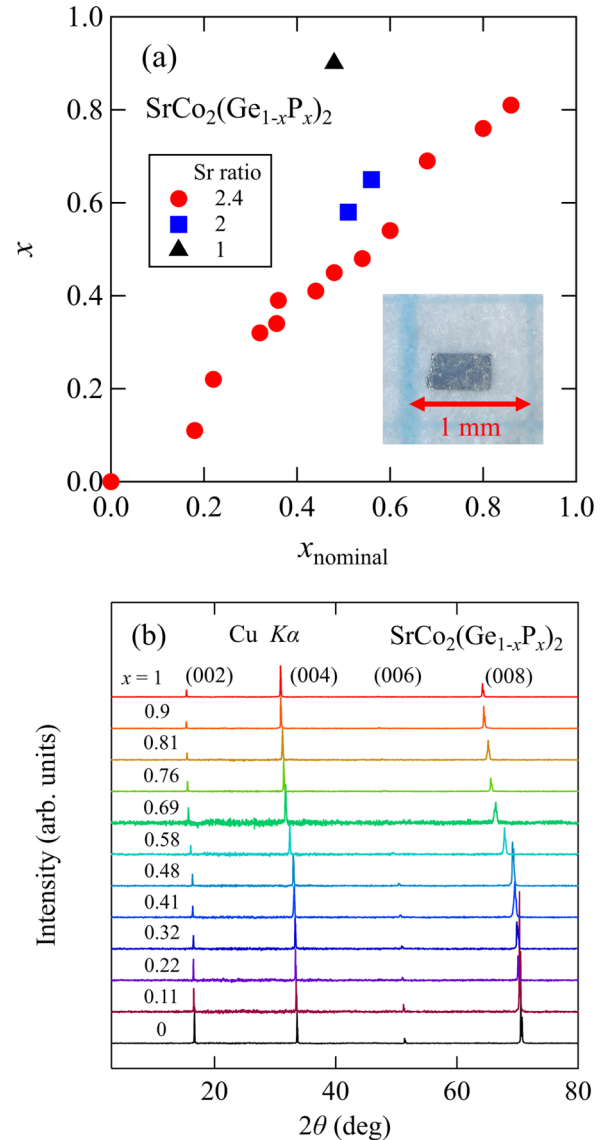
FIG. 1. (a) Plots of the P content x determined using EDX measurements against the starting P content $x_{nominal}$. The plots are distinguished by different markers depending on starting Sr ratio. The inset is the photograph of a $SrCo_2(Ge_{1-x}P_x)_2$ single crystal. (b) X-ray diffraction patterns of $SrCo_2(Ge_{1-x}P_x)_2$ single crystals. The spectra are normalized using the intensity of each (004) diffraction peak. Only (00l) reflections are observed, which suggests that the plate surface is perpendicular to the c axis.

under a magnetic field of 1 T for $H \parallel ab$. Although $\chi(T)$ for $0 \leqslant x \leqslant 0.22$ shows a nearly temperature-independent Pauli paramagnetic behavior, $\chi(T)$ for $x \geqslant 0.34$ at high temperatures follows the Curie-Weiss law with a temperature-independent term χ_0. The temperature dependence of $1/(\chi - \chi_0)$ is shown in Fig. 2(b). The estimated effective magnetic moment μ_{eff} and the Weiss temperature θ will be discussed in Sec. III F.

For $0.39 \leqslant x \leqslant 0.58$, $1/(\chi - \chi_0)$ shows ferromagnetic behavior at low temperatures. Assuming that the y-axis intercept of the linear extrapolation of the Arrott plots is the square of the spontaneous magnetization, a finite spontaneous
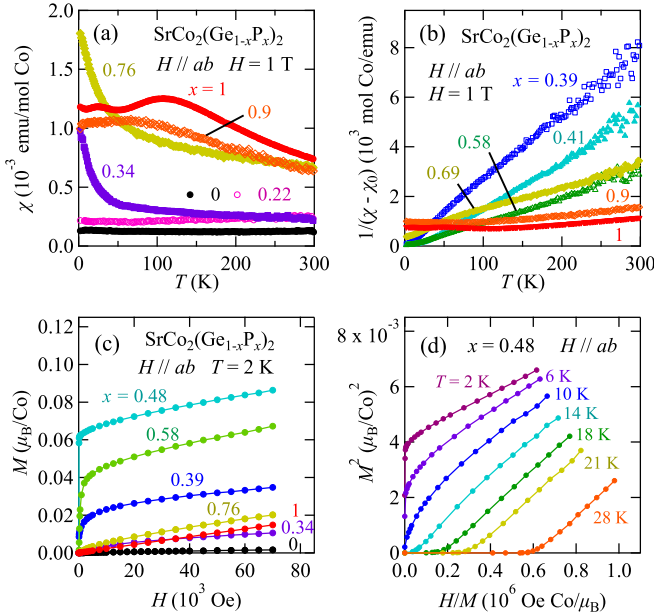
FIG. 2. Magnetic properties of $SrCo_2(Ge_{1-x}P_x)_2$. (a) Temperature dependence of the magnetic susceptibility under a magnetic field of 1 T for $H \parallel ab$. (b) Temperature dependence of the inverse of the magnetic susceptibility. The temperature independent term χ_0 estimated by fitting $\chi(T)$ with the Curie-Weiss formula has been subtracted. (c) Isothermal magnetization curves measured at 2 K under a magnetic field up to 7 T for $H \parallel ab$. (d) Arrott plot for $x = 0.48$.

magnetization exists at 2 K only for these compositions. These results are roughly consistent with the previous study on polycrystalline samples [9]. In the ferromagnetic phase, the magnetic easy plane is the ab plane (see Fig. 1 in the Supplemental Material [27]).

As x approaches 1, a broad maximum of $\chi(T)$ appears. Considering that $SrCo_2P_2$ ($x = 1$) exhibits an itinerant-electron metamagnetic transition at $H = 59.7$ T [4], it is suggested that the maximum of $\chi(T)$ in this system is a common feature that is observed in nearly ferromagnetic metals showing metamagnetic transition, such as YCo_2 [13,31], $LaCo_9Si_4$ [32], and Co_3Mo_3C [33]. For $x = 1$, an additional anomaly at $T = 30$ K can be seen as in the previous studies [4,34]. Although its origin remains unclear, it might be attributed to a crossover between two magnetic states [4].

Figure 2(d) shows the Arrott plot for $x = 0.48$. The plots show a good linearity at 2 K, whereas they show concave curvatures around T_C. In the simple mean-field theory, the Arrott plot would show linear behavior around T_C implying that the sixth and higher terms of the Landau expansion of the free energy $F(M)$ are neglected. In the present case, the contribution of the higher terms is not negligible, i.e., the effect of spin fluctuations must be considered. In order to characterize the feature of the ferromagnetic phase, we estimated the critical exponents from the magnetization data, which will be discussed in Sec. III C.

C. Critical exponents

The critical behavior of a second-order ferromagnetic transition is characterized using the critical exponents β, γ, and
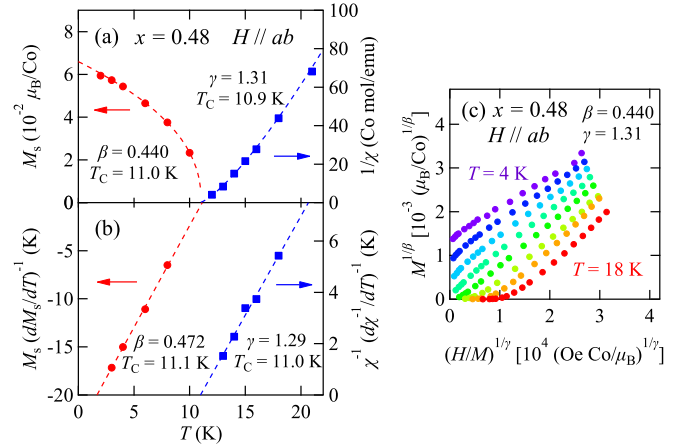
FIG. 3. (a) Temperature dependence of the spontaneous magnetization M_s (red circles) and the reciprocal susceptibility $1/\chi$ (blue squares) for $x = 0.48$. The dashed lines are the fitting curves. (b) Kouvel-Fisher plots of $M_s(dM_s/dT)^{-1}$ (red circles) and $\chi^{-1}(d\chi^{-1}/dT)^{-1}$ (blue squares). The dashed lines are the linear fits. (c) $M^{1/\beta}$ vs $(H/M)^{1/\gamma}$ plots within a temperature range of 4–18 K at a step of 2 K. The adopted parameters $\beta = 0.440$ and $\gamma = 1.31$ were obtained using the modified Arrott plot method.

δ [35]. They are associated with the temperature dependence of the spontaneous magnetization $M_s(T)$ below T_C, the temperature dependence of the reciprocal susceptibility $\chi^{-1}(T)$ above T_C and the isothermal magnetization $M(H)$ at T_C, respectively, as the following equations:

$$M_s(T) = M_s(0)(-\varepsilon)^\beta, \quad \varepsilon < 0, \tag{1}$$

$$\chi^{-1}(T) = (h_0/m_0)\varepsilon^\gamma, \quad \varepsilon > 0, \tag{2}$$

$$M(H) = DH^{1/\delta}, \quad \varepsilon = 0, \tag{3}$$

where $\varepsilon = (T - T_C)/T_C$ is the reduced temperature and h_0/m_0 and D are the critical amplitudes [36]. In order to evaluate β and γ, we adopt the modified Arrott plot method described in Ref. [11]. Figure 3(a) shows an example for $x = 0.48$. The obtained exponents are $\beta = 0.440$ and $\gamma = 1.31$. These values are close to those predicted in the SCR theory for three-dimensional (3D) itinerant ferromagnets near a quantum critical point ($\beta = 0.5$, $\gamma = 4/3$) [24,37]. A small difference in β may reflect a quasi-two-dimensional feature of CoX layers.

To validate the obtained critical exponents, we also estimate the exponents using the Kouvel-Fisher method [38]. Differentiating both sides in Eqs. (1) and (2) by temperature, the following equations are derived:

$$M_s(T)\left[\frac{d}{dT}M_s(T)\right]^{-1} = \frac{T - T_C}{\beta}, \tag{4}$$

$$\chi^{-1}(T)\left[\frac{d}{dT}\chi^{-1}(T)\right]^{-1} = \frac{T - T_C}{\gamma}. \tag{5}$$

Therefore, the plots of $M_s(T)[dM_s(T)/dT]^{-1}$ vs T and $\chi^{-1}(T)[d\chi^{-1}(T)/dT]^{-1}$ vs T are expected to be linear, and the slopes correspond $1/\beta$ and $1/\gamma$, respectively. As shown in Fig. 3(b), the plots exhibit a good linearity, and the linear

fits give $\beta = 0.472$, $\gamma = 1.29$. These values are close to the results of the modified Arrott plot method.

In addition, the exponent δ can be estimated using the Widom scaling law $\delta = 1 + \gamma/\beta$ [39]. Using the values of β and γ estimated from the modified Arrott plots and the Kouvel-Fisher plots, we obtain $\delta = 3.98$ and $\delta = 3.83$, respectively. The obtained values are larger than 3 of the mean-field theory, which suggests that the contribution of the sixth- and higher-order terms of the Landau expansion of the free-energy $F(M)$ is not negligible in $SrCo_2(Ge_{1-x}P_x)_2$. Figure 3(c) shows $M^{1/\beta}$ vs $(H/M)^{1/\gamma}$ for $x = 0.48$ constructed using the critical exponents estimated from the modified Arrott plots. The plots show a good linearity around T_C.

D. Evaluation of spin fluctuations

As discussed in Sec. III C, it is reasonable to characterize the ferromagnetism in this system using the theory of spin fluctuations in itinerant-electron magnets. The large δ value suggests that the fourth term of the Landau expansion $F(M)$ becomes small near T_C. According to Takahashi, if one assumes a conservation of the total amplitude of zero-point and thermal spin fluctuations against temperature, the fourth term in the Landau expansion corresponds to the temperature-depending zero-point spin fluctuations [40]. In this framework, the temperature dependence of the spontaneous magnetization $M_s(T)$ at low temperatures is expressed as

$$\left(\frac{M_s(T)}{M_s(0)}\right)^2 = 1 - \frac{50.4}{p_s^4}\left(\frac{T}{T_A}\right)^2, \tag{6}$$

where p_s is the spontaneous magnetization in Bohr magneton unit, and T_A is the spin-fluctuation parameter corresponding to the local amplitude of spin fluctuations in the wave vector space. As shown in Fig. 4, the spontaneous magnetization estimated using the modified Arrott plots almost satisfies Eq. (6) at low temperatures. In addition, the spin-fluctuation parameter $\bar{F}_1$ corresponding to the strength of the mode-mode coupling between spin fluctuations can be estimated from the Arrott plot at the lowest temperature as the following equation:

$$\bar{F}_1 = \frac{16\mu_B}{\eta k_B}, \tag{7}$$

where μ_B is the Bohr magneton in the units of J/T and η is the gradient of the Arrott plot in the units of $(\mu_B/\text{atom})^3 \, T^{-1}$ [40]. Then, the relationship between the spin-fluctuation parameters is written as

$$\bar{F}_1 = \frac{4}{15}\frac{k_B T_A^2}{T_0}, \tag{8}$$

where T_0 corresponds to the energy width of the dynamical spin fluctuation spectrum [40]. The spin-fluctuation parameters estimated from Eqs. (6)–(8) are summarized in Table I. The obtained values of T_A, T_0, and $\bar{F}_1$ are close to those in typical itinerant-electron ferromagnets (approximately 10^3–10^4, 10^2–10^3, and 10^4–10^5 K, respectively [15,41–47]). The parameters satisfy the generalized Rhodes-Wohlfarth relation $p_{\text{eff}}/p_s = 1.4(T_C/T_0)^{-2/3}$ in the 3D ferromagnetic system proposed by Takahashi [40], which suggests that the obtained
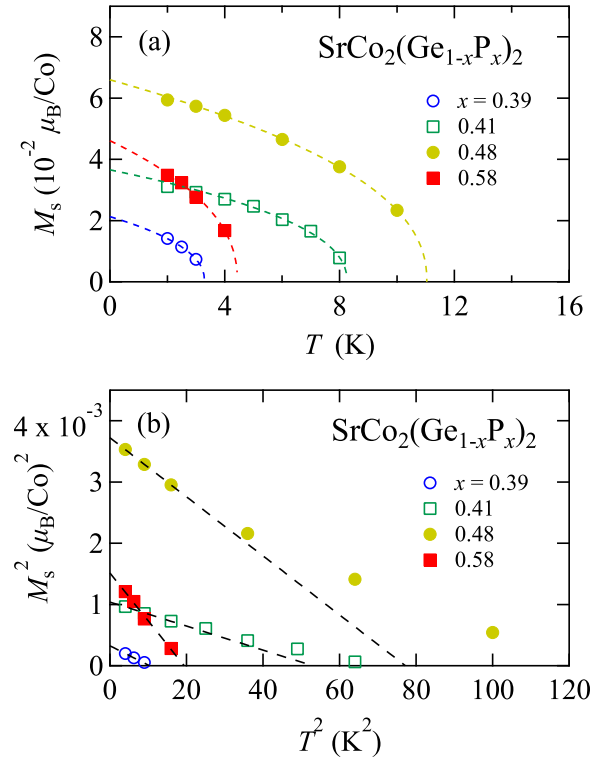
FIG. 4. (a) Temperature dependence of the spontaneous magnetization M_s for $x = 0.39$, 0.41, 0.48, and 0.58. The dashed lines are the fitting curves obtained using the modified Arrott plot method. (b) M_s^2 vs T^2 plots. The dashed lines are the linear fits at low temperatures.

parameters are consistent in this framework (see Fig. 2 in the Supplemental Material [27]).

According to the SCR theory, the Curie temperature T_C can be calculated using T_A, T_0, and p_s, as the following equation:

$$T_C = (60c)^{-3/4} p_s^{3/2} T_A^{3/4} T_0^{1/4} \quad (c = 0.3353). \tag{9}$$

The calculated values of T_C are 5.3, 9.4, 9.6, and 5.8 K for $x = 0.39$, 0.41, 0.48, and 0.58, respectively. They are almost consistent with the experimental values estimated from the modified Arrott plots (3.3, 8.2, 11.0, and 4.4 K, respectively).

These results suggest that the ferromagnetism in this system can be understood in the framework of the theory of spin fluctuations for weak itinerant ferromagnets. However, there is a finite ambiguity in the obtained value of T_A since the Curie temperature is too low to accurately evaluate the temperature derivative of the spontaneous magnetization as shown in Fig. 4. Owing to such an ambiguity, the reciprocal susceptibilities calculated using the obtained parameters are

TABLE I. Spin-fluctuation parameters of $SrCo_2(Ge_{1-x}P_x)_2$ estimated from the magnetization data using Takahashi's theory.

x	T_A (K)	T_0 (K)	$\bar{F}_1$ (K)
0.39	7.02×10^4	537	2.45×10^6
0.41	4.97×10^4	463	1.42×10^6
0.48	1.68×10^4	282	2.66×10^5
0.58	2.07×10^4	294	3.87×10^5
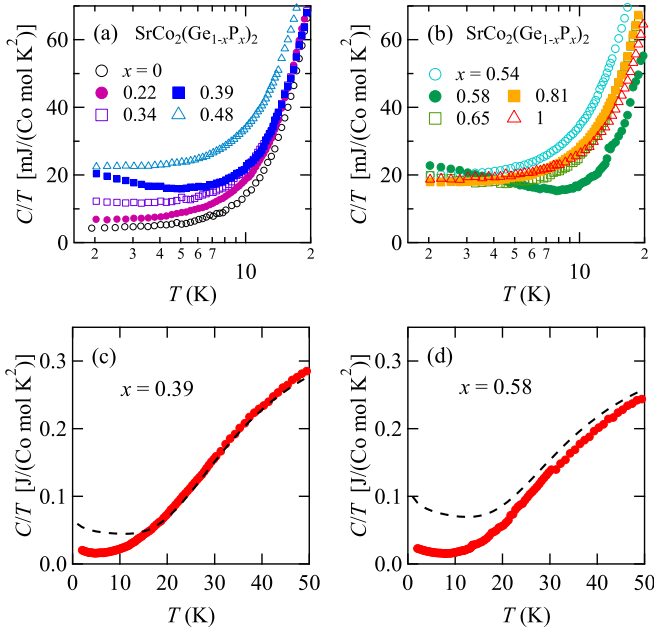
FIG. 5. Specific heats in $SrCo_2(Ge_{1-x}P_x)_2$. (a) and (b) C/T as a function of temperature on a logarithmic scale for (a) $0 \leqslant x \leqslant 0.48$ and (b) $0.54 \leqslant x \leqslant 1$. (c) and (d) Temperature dependence of C/T for (c) $x = 0.39$ and (d) $x = 0.58$. The dashed lines indicate the calculated C/T described in the text.

FIG. 6. Lattice parameter ratio c/a in $SrCo_2(Ge_{1-x}P_x)_2$ (red circles), $Ca_{1-x}Sr_xCo_2P_2$ (blue squares) and $Ca_{1-x}Eu_xCo_2P_2$ (green triangles). The data for $Ca_{1-x}Sr_xCo_2P_2$ is cited from Ref. [4]. The dashed lines indicate the cT or ucT phase, and the solid lines indicate the intermediate phase for each system.

larger than the experimental results (see Fig. 3 in the Supplemental Material [27]).

E. Quantum critical phenomena in heat capacity

Figures 5(a) and 5(b) show C/T as a function of the temperature on a logarithmic scale for $0 \leqslant x \leqslant 0.48$ and $0.54 \leqslant x \leqslant 1$, respectively. Since the magnetic moment of Co is very small, no anomaly corresponding to the ferromagnetic ordering can be seen. In all compounds except for $x = 0.39$ and 0.58, C/T is almost constant at low temperatures. In both $x = 0.39$ and 0.58, C/T exhibits a distinct upturn proportional to $\ln T$. According to the SCR theory, such an upturn can be detected only in the vicinity of quantum critical point, and the temperature dependence of the specific heat derived from spin fluctuations is expressed as

$$\frac{C_m}{T} \simeq \frac{9N_0}{T_0} \int_0^{1/K_0} dx\, x^2 \frac{1}{t}\left[-u - \frac{1}{2} + u^2\Psi'(u)\right], \quad (10)$$

$$t = T/T_0 K_0^3, \quad (11)$$

$$K_0^2 = 1/2\alpha T_A \chi(0), \quad (12)$$

$$u = x[x^2 + \chi(0)/\chi(T)]/t \simeq x(x^2 + 1)/t, \quad (13)$$

where N_0 is the number of magnetic atoms, $\Psi'(u)$ the trigamma function, and $(1 - \alpha)^{-1}$ the Stoner enhancement factor [48]. For systems near a ferromagnetic ordering, α is often approximated as 1. T_0 and T_A are the spin-fluctuation parameters. Although the calculation of C_m/T using the formula described above has a quantitative ambiguity due to the neglection of low-energy excitations derived from minor dispersions of spin fluctuation unique to each compound, an

upturn at low temperatures would be qualitatively reproduced when the parameters for quantum critical point are assigned.

We calculated C_m/T for both $x = 0.39$ and 0.58 with Eqs. (10)–(13) using the parameters estimated from the magnetization data (shown in Table I). In addition, we also estimated the lattice specific heat by fitting C/T at high temperatures with the sum of Debye and Einstein contributions. The dashed lines in Figs. 5(c) and 5(d) show the sum of the calculated magnetic contribution and the estimated lattice contribution. The upturn at low temperatures is qualitatively reproduced. The fact that upturns are observed at both $x = 0.39$ and 0.58 suggests the existence of two independent ferromagnetic critical points near these compositions.

F. Magnetic phase diagram

The structural transition between the cT and ucT phases is identified using the lattice parameter ratio c/a. Figure 6 shows the composition dependence of c/a for $SrCo_2(Ge_{1-x}P_x)_2$ (red circles). As a comparison, the data for $Ca_{1-x}Eu_xCo_2P_2$ (green triangles) and $Ca_{1-x}Sr_xCo_2P_2$ (blue squares, cited from Ref. [4]) are also shown. $CaCo_2P_2$ and $EuCo_2P_2$ have been identified as having the cT and ucT structures, respectively [49,50]. For $Ca_{1-x}Eu_xCo_2P_2$, c/a increases slightly for $0 \leqslant x < 0.5$ and for $0.5 < x \leqslant 1$. The change of c/a at $x = 0.5$ is steplike, which suggests that the structural transition between the cT and ucT phases is first-order. For $SrCo_2(Ge_{1-x}P_x)_2$ and $Ca_{1-x}Sr_xCo_2P_2$, there is a finite composition range where the variation of c/a is relatively steep (shown as solid lines) in addition to the ranges where c/a increases slightly (shown as dashed lines). This implies that the first-order structural transition is broadened owing to a disorder caused by elemental substitution. This intermediate region is denoted as the intermediate phase to distinguish it from the cT and ucT phases. According to the recent μ^+SR study on $Ca_{1-x}Sr_xCo_2P_2$, the antiferromagnetic behavior for
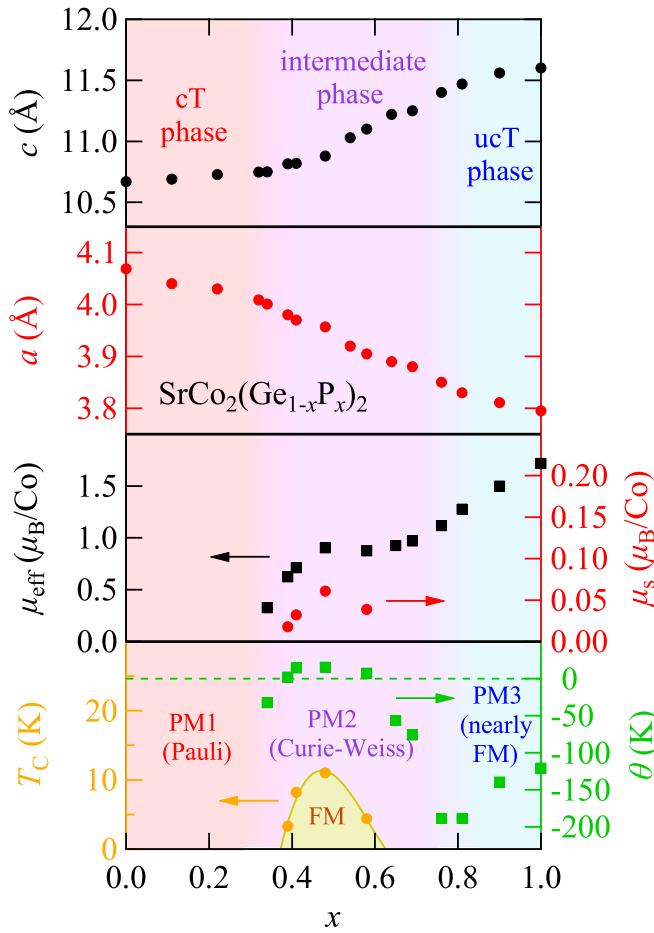
FIG. 7. Lattice and magnetic parameters in $SrCo_2(Ge_{1-x}P_x)_2$. The lattice parameters c and a are shown in the upper and second panels, respectively. The effective magnetic moment μ_{eff} (black squares) and the spontaneous magnetic moment μ_s (red circles) are shown in the third panel. The Weiss temperature θ (green squares) and the Curie temperature T_C (yellow circles) are shown in the bottom panel. FM and PM stand for the ferromagnetic state and the paramagnetic state, respectively.

$0.25 \leqslant x \leqslant 0.52$ is attributed not to a long-range order but to a short-range order [51], which is consistent with the present identification of the structural phase. For $SrCo_2(Ge_{1-x}P_x)_2$, the composition range of the intermediate phase is highly wider than that for $Ca_{1-x}Sr_xCo_2P_2$, owing to the destabilization of the cT and ucT phases caused by a randomness in the X atoms which have a role to form the interlayer X-X bonds. The existence of the wide intermediate phase is closely related to the anomalous magnetic properties, which is discussed below.

Figure 7 shows the phase diagram of $SrCo_2(Ge_{1-x}P_x)_2$. For $x < 0.34$, the lattice parameter c is almost constant, suggesting that the system is in the cT phase. In this region, the magnetic susceptibility exhibits a nearly temperature-independent Pauli paramagnetic (PM) behavior. This phase is denoted as PM1.

For $0.34 \leqslant x \leqslant 0.81$, the system has the intermediate structure described above, although the boundary between the intermediate and ucT phases is not very clear. The magnetic susceptibility follows the Curie-Weiss law at high temperatures, which is completely different from the behavior in PM1.

This paramagnetic phase is denoted as PM2. According to the SCR theory, the Curie-Weiss-like behavior of the magnetic susceptibility in itinerant-electron magnets is attributed to the temperature dependence of the thermal spin fluctuations [24]. In this framework, the effective magnetic moment μ_{eff} corresponds not to the magnitude of the magnetic moment but to the amplitude of the local spin fluctuations. The μ_{eff} increases with P substitution for $x < 0.48$, whereas that for $0.48 \leqslant x \leqslant 0.81$ is almost constant. The ratios of μ_{eff} to μ_s are 34.7, 22.1, 14.8, and 22.5 for $x = 0.39, 0.41, 0.48$, and 0.58, respectively. The values larger than 1 are typical in itinerant ferromagnetic compounds. The Curie temperatures for ferromagnetic samples are quite lower than in the previous study on polycrystals [9], which is owing to the difference in the estimation methods. T_C shown in Fig. 7 is determined carefully analyzing the magnetization curves using the modified Arrott plots, whereas the previously reported values have been obtained assuming $M(T_C) = 20 \pm 10\% M (2 \text{ K})$ for $M(T)$ at $H = 1$ T. The estimation of the Curie temperatures of weak ferromagnets is strongly affected by the magnetic-field dependence of magnetization, so the present values should be more accurate.

For $x > 0.81$, the lattice parameters are nearly constant, which suggests that the system is in the ucT phase. In this region, the temperature dependence of the magnetic susceptibility exhibits a maximum as with nearly ferromagnetic metals. This phase is denoted as PM3. Probably owing to lattice defects induced by chemical substitution and X-X bond formation, such a maximum behavior cannot be observed in PM2.

In the case of itinerant-electron magnets with ferromagnetic spin fluctuations, the absolute value of the Weiss temperature $|\theta|$ indicates the distance from the ferromagnetic quantum critical point [24,52]. The sign of θ is switched around $x = 0.38$ and 0.6, which is consistent with the fact that ferromagnetic quantum critical phenomena are observed at both $x = 0.39$ and 0.58 in specific-heat measurements.

Next, we discuss the origin of the quantum critical phase transition in $SrCo_2(Ge_{1-x}P_x)_2$. The quantum critical point approximately at $x = 0.58$ exists inside the structural intermediate phase. In the vicinity of this critical point, μ_{eff} remains almost constant whereas θ decreases with P substitution, which suggests the variation in the ferromagnetic interaction drives the quantum critical phase transition. In fact, the parameter T_A corresponding to the local amplitude of spin fluctuations at $\mathbf{Q} = 0$ (ferromagnetic spin fluctuations) decreases from $x = 0.39$ to 0.58 as shown in Table I. These results are consistent with the prediction in the SCR theory for ferromagnetic quantum critical region [24]. The intralayer Co-Co distance (equal to $a/\sqrt{2}$) decreases gradually with P substitution, which can lead to a gradual reduction of ferromagnetic interaction.

On the other hand, for near $x = 0.39$, both the electronic specific heat and effective magnetic moment increase markedly with increasing x as shown in Figs. 5(a) and 7, respectively. A similar behavior has been observed in $FeGa_{3-x}Ge_x$ in which changes in the Fe-3d-Ga-4p hybridization due to Ge substitution are considered to be the origin of quantum critical phase transition [20,53]. In the present case, the quantum phase transition at $x = 0.39$ can be attributed to a

steep increase in the density of states at the Fermi level, which is driven by the structural change from the cT to the intermediate phase. The temperature dependence of the resistivity for $x = 0.39$ and 0.65 also suggests that the two independent quantum critical points have different origins (see Fig. 4 in the Supplemental Material [27]).

Although the present results suggest that the ferromagnetic quantum criticality is closely related to the existence of the intermediate phase, the compositional variation in spin fluctuations for the paramagnetic region remains to be revealed. It is a future issue to evaluate spin fluctuations in a wide range of compositions including the PM1 and PM3 phase, using NMR measurements and other techniques.

IV. CONCLUSION

We studied the physical properties of single crystals of $SrCo_2(Ge_{1-x}P_x)_2$ by means of magnetization and specific heat measurements. Although the compounds in the cT and ucT phases show no signs of magnetic ordering, those with $0.39 \leqslant x \leqslant 0.58$ exhibit ferromagnetism at low temperatures. The critical exponents of the ferromagnetic transition are close to those predicted in the SCR theory for itinerant ferromagnets. We found that an intermediate phase exists for a wide range of composition, which induces ferromagnetic quantum critical phenomena in $SrCo_2(Ge_{1-x}P_x)_2$. The present results possibly promote further research on novel quantum properties of itinerant-electron magnetism.

[1] F. Steglich, J. Aarts, C. D. Bredl, W. Lieke, D. Meschede, W. Franz, and H. Schäfer, Superconductivity in the Presence of Strong Pauli Paramagnetism: $CeCu_2Si_2$, Phys. Rev. Lett. **43**, 1892 (1979).

[2] M. Rotter, M. Tegel, and D. Johrendt, Superconductivity at 38 K in the Iron Arsenide $(Ba_{1-x}K_x)Fe_2As_2$, Phys. Rev. Lett. **101**, 107006 (2008).

[3] S. Kasahara, H. J. Shi, K. Hashimoto, S. Tonegawa, Y. Mizukami, T. Shibauchi, K. Sugimoto, T. Fukuda, T. Terashima, Andriy H. Nevidomskyy, and Y. Matsuda, Electronic nematicity above the structural and superconducting transition in $BaFe_2(As_{1-x}P_x)_2$, Nature (London) **486**, 382 (2012).

[4] M. Imai, C. Michioka, H. Ohta, A. Matsuo, K. Kindo, H. Ueda, and K. Yoshimura, Anomalous itinerant-electron metamagnetic transition in the layered $Sr_{1-x}Ca_xCo_2P_2$ system, Phys. Rev. B **90**, 014407 (2014).

[5] M. Reehuis, W. Jeitschko, M. H. Möller, and P. J. Brown, A neutron diffraction study of the magnetic structure of $EuCo_2P_2$, J. Phys. Chem. Solids **53**, 687 (1992).

[6] M. Chefki, M. M. Abd-Elmeguid, H. Micklitz, C. Huhnt, W. Schlabitz, M. Reehuis, and W. Jeitschko, Pressure-induced Transition of the Sublattice Magnetization in $EuCo_2P_2$: Change from Local Moment $Eu(4f)$ to Itinerant $Co(3d)$ Magnetism, Phys. Rev. Lett. **80**, 802 (1998).

[7] S. Jia, A. J. Williams, P. W. Stephens, and R. J. Cava, Lattice collapse and the magnetic phase diagram of $Sr_{1-x}Ca_xCo_2P_2$, Phys. Rev. B **80**, 165107 (2009).

[8] R. Hoffmann and C. Zheng, Making and breaking bonds in the solid state: The $ThCr_2Si_2$ structure, J. Phys. Chem. **89**, 4175 (1985).

[9] S. Jia, P. Jiramongkolchai, M. R. Suchomel, B. H. Toby, J. G. Checkelsky, N. P. Ong, and R. J. Cava, Ferromagnetic quantum critical point induced by dimer-breaking in $SrCo_2(Ge_{1-x}P_x)_2$, Nat. Phys. **7**, 207 (2011).

[10] A. Arrott and J. Noakes, Approximate Equation of State For Nickel Near its Critical Temperature, Phys. Rev. Lett. **19**, 786 (1967).

[11] Y. Liu, V. N. Ivanovski, and C. Petrovic, Critical behavior of the van der Waals bonded ferromagnet $Fe_{3-x}GeTe_2$, Phys. Rev. B **96**, 144429 (2017).

[12] T. N. Lamichhane, L. Xiang, Q. Lin, T. Pandey, D. S. Parker, T.-H. Kim, L. Zhou, M. J. Kramer, S. L. Bud'ko, and P. C. Canfield, Magnetic properties of single crystalline itinerant ferromagnet $AlFe_2B_2$, Phys. Rev. Mater. **2**, 084408 (2018).

[13] K. Yoshimura, T. Shimizu, M. Takigawa, H. Yasuoka, and Y. Nakamura, Nuclear magnetic relaxation in nearly ferromagnetic YCo_2, J. Phys. Soc. Jpn. **53**, 503 (1984).

[14] K. Yoshimura and Y. Nakamura, New weakly itinerant ferromagnetic system, $Y(Co_{1-X}Al_X)_2$, Solid State Commun. **56**, 767 (1985).

[15] K. Yoshimura, M. Takigawa, Y. Takahashi, H. Yasuoka, and Y. Nakamura, NMR study of weakly itinerant ferromagnetic $Y(Co_{1-x}Al_x)_2$, J. Phys. Soc. Jpn. **56**, 1138 (1987).

[16] K. Yoshimura, M. Mekata, M. Takigawa, Y. Takahashi, and H. Yasuoka, Spin fluctuations in $Y(Co_{1-x}Al_x)_2$: A transition system from nearly to weakly itinerant ferromagnetism, Phys. Rev. B **37**, 3593 (1988).

[17] K. Yoshimura, T. Imai, T. Kiyama, K. R. Thurber, A. W. Hunt, and K. Kosuge, ^{17}O NMR Observation of Universal Behavior of Ferromagnetic Spin Fluctuations in the Itinerant Magnetic System $Sr_{1-x}Ca_xRuO_3$, Phys. Rev. Lett. **83**, 4397 (1999).

[18] T. Kiyama, K. Yoshimura, K. Kosuge, H. Mitamura, and T. Goto, High-field magnetization of $Sr_{1-x}Ca_xRuO_3$, J. Phys. Soc. Jpn. **68**, 3372 (1999).

[19] Y. Itoh, T. Mizoguchi, and K. Yoshimura, Novel critical exponent of magnetization curves near the ferromagnetic quantum phase transitions of $Sr_{1-x}A_xRuO_3 (A = Ca, La_{0.5}Na_{0.5}, and La)$, J. Phys. Soc. Jpn. **77**, 123702 (2008).

[20] K. Umeo, Y. Hadano, S. Narazu, T. Onimaru, M. A. Avila, and T. Takabatake, Ferromagnetic instability in a doped band gap semiconductor $FeGa_3$, Phys. Rev. B **86**, 144421 (2012).

[21] M. Majumder, M. Wagner-Reetz, R. Cardoso-Gil, P. Gille, F. Steglich, Y. Grin, and M. Baenitz, Towards ferromagnetic quantum criticality in $FeGa_{3-x}Ge_x$: ^{71}Ga NQR as a zero-field microscopic probe, Phys. Rev. B **93**, 064410 (2016).

[22] J. Munevar, M. Cabrera-Baez, M. Alzamora, J. Larrea, E. M. Bittar, E. Baggio-Saitovitch, F. J. Litterst, R. A. Ribeiro, M. A. Avila, and E. Morenzoni, Magnetic order of intermetallic FeGa$_{3-y}$Ge$_y$ studied by μSR and ^{57}Fe Mössbauer spectroscopy, Phys. Rev. B **95**, 125138 (2017).

[23] K. Rana, H. Kotegawa, R. R. Ullah, J. S. Harvey, S. L. Bud'ko, P. C. Canfield, H. Tou, V. Taufour, and Y. Furukawa, Magnetic fluctuations in the itinerant ferromagnet LaCrGe$_3$ studied by ^{139}La NMR, Phys. Rev. B **99**, 214417 (2019).

[24] T. Moriya, *Spin Fluctuations in Itinerant Electron Magnetism* (Springer-Verlag, Berlin/Heidelberg, 1985), Vol. 56.

[25] M. Reehuis, C. Ritter, R. Ballou, and W. Jeitschko, Ferromagnetism in the ThCr$_2$Si$_2$ type phosphide LaCo$_2$P$_2$, J. Magn. Magn. Mater. **138**, 85 (1994).

[26] W. Kraus and G. Nolze, POWDER CELL - a program for the representation and manipulation of crystal structures and calculation of the resulting x-ray powder patterns, J. Appl. Cryst. **29**, 301 (1996).

[27] See Supplemental Material at http://link.aps.org/supplemental/10.1103/PhysRevB.107.134427 for further details of physical properties and the results of numerical calculations of the reciprocal susceptibility. The Supplemental Material also contains Refs. [28–30].

[28] M. Imai, C. Michioka, H. Ueda, and K. Yoshimura, Static and dynamical magnetic properties of the itinerant ferromagnet LaCo$_2$P$_2$, Phys. Rev. B **91**, 184414 (2015).

[29] T. Sakakibara, T. Goto, K. Yoshimura, M. Shiga, and Y. Nakamura, Itinerant electron metamagnetism in Y(Co$_{1-x}$Al$_x$)$_2$, Phys. Lett. A **117**, 243 (1986).

[30] K. Ueda and T. Moriyia, Contribution of spin fluctuations to the electrical and thermal resistivities of weakly and nearly ferromagnetic metals, J. Phys. Soc. Jpn. **39**, 605 (1975).

[31] S. Hirosawa and Y. Nakamura, Knight shift of ^{59}Co in RCo$_2$(R = Y, Pr, Er and Tm), J. Phys. Soc. Jpn. **51**, 2464 (1982).

[32] H. Michor, M. El-Hagary, M. D. Mea, M. W. Pieper, M. Reissner, G. Hilscher, S. Khmelevskyi, P. Mohn, G. Schneider, G. Giester, and P. Rogl, Itinerant electron metamagnetism in LaCo$_9$Si$_4$, Phys. Rev. B **69**, 081404(R) (2004).

[33] T. Waki, Y. Umemoto, S. Terazawa, Y. Tabata, A. Kondo, K. Sato, K. Kindo, S. Alconchel, F. Sapiña, Y. Takahashi, and H. Nakamura, Itinerant electron metamagnetism in η-carbide-type compound Co$_3$Mo$_3$C, J. Phys. Soc. Jpn. **79**, 093703 (2010).

[34] A. Teruya, A. Nakamura, T. Takeuchi, H. Harima, K. Uchima, M. Hedo, T. Nakama, and Y. Ōnuki, De Haas–van Alphen effect and Fermi surface properties in nearly ferromagnet SrCo$_2$P$_2$, J. Phys. Soc. Jpn. **83**, 113702 (2014).

[35] H. E. Stanley, *Introduction to Phase Transitions and Critical Phenomena* (Oxford University Press, London/New York, 1971).

[36] M. E. Fisher, The theory of equilibrium critical phenomena, Rep. Prog. Phys. **30**, 615 (1967).

[37] A. J. Millis, Effect of a nonzero temperature on quantum critical points in itinerant fermion systems, Phys. Rev. B **48**, 7183 (1993).

[38] J. S. Kouvel and M. E. Fisher, Detailed magnetic behavior of nickel near its Curie point, Phys. Rev. **136**, A1626 (1964).

[39] B. Widom, Equation of state in the neighborhood of the critical point, J. Chem. Phys. **43**, 3898 (1965).

[40] Y. Takahashi, On the origin of the Curie-Weiss law of the magnetic susceptibility in itinerant electron ferromagnetism, J. Phys. Soc. Jpn. **55**, 3553 (1986).

[41] D. Bloch, J. Voiron, V. Jaccarino, and J. H. Wernick, The high field-high pressure magnetic properties of MnSi, Phys. Lett. A **51**, 259 (1975).

[42] F. R. de Boer, C. J. Schinkel, J. Biesterbos, and S. Proost, Exchange-enhanced paramagnetism and weak ferromagnetism in the Ni$_3$Al and Ni$_3$Ga phases; Giant moment inducement in Fe-doped Ni$_3$Ga, J. Appl. Phys. **40**, 1049 (1969).

[43] J. Takeuchi and Y. Masuda, Low temperature specific heat of itinerant electron ferromagnet Sc$_3$In, J. Phys. Soc. Jpn. **46**, 468 (1979).

[44] S. Ogawa, Electrical resistivity of weak itinerant ferromagnet ZrZn$_2$, J. Phys. Soc. Jpn. **40**, 1007 (1976).

[45] K. Shimizu, H. Maruyama, H. Yamazaki, and H. Watanabe, Effect of spin fluctuations on magnetic properties and thermal expansion in pseudobinary system Fe$_x$Co$_{1-x}$Si, J. Phys. Soc. Jpn. **59**, 305 (1990).

[46] J. Beille, D. Bloch, and M. J. Besnus, Itinerant ferromagnetism and susceptibility of nickel-platinum alloys, J. Phys. F: Met. Phys. **4**, 1275 (1974).

[47] A. Fujita, K. Fukamichi, H. A. Katori, and T. Goto, Spin fluctuations in amorphous La(Ni$_x$Al$_{1-x}$)$_{13}$ alloys consisting of icosahedral clusters, J. Phys.: Condens. Matter **7**, 401 (1995).

[48] R. Konno and T. Moriya, Quantitative aspects of the theory of nearly ferromagnetic metals, J. Phys. Soc. Jpn. **56**, 3270 (1987).

[49] A. Mewis, Ternäre phosphide mit ThCr$_2$Si$_2$ -struktur / Ternary phosphides with the ThCr$_2$Si$_2$ Structure, Z. Naturforsch., B: J. Chem. Sci. **35**, 141 (1980).

[50] R. Marchand and W. Jeitschko, Ternary lanthanoid-transition metal pnictides with ThCr$_2$Si$_2$-type structure, J. Solid State Chem. **24**, 351 (1978).

[51] J. Sugiyama, H. Nozaki, I. Umegaki, M. Harada, Y. Higuchi, K. Miwa, E. J. Ansaldo, J. H. Brewer, M. Imai, C. Michioka, K. Yoshimura, and M. Månsson, Variation of magnetic ground state of Sr$_{1-x}$Ca$_x$Co$_2$P$_2$ determined with μ^+SR, Phys. Rev. B **91**, 144423 (2015).

[52] A. Ishigaki and T. Moriya, Nuclear magnetic relaxation around the magnetic instabilities in metals, J. Phys. Soc. Jpn. **65**, 3402 (1996).

[53] Y. Zhang, J.-S. Chen, J. Mac, J. Nie, M. Imai, C. Michioka, Y. Hadanoh, M. A. Avilai, T. Takabatake, S. Lie, and K. Yoshimura, Transitions from a Kondo-like diamagnetic insulator into a modulated ferromagnetic metal in FeGa$_{3-y}$Ge$_y$, Proc. Natl. Acad. Sci. USA **115**, 3273 (2018).